Journal of Alloys and Compounds 506 (2010) 928–939

Contents lists available at ScienceDirect

Journal of Alloys and Compounds

journal homepage: www.elsevier.com/locate/jallcom

The effects of nanometric nickel (n-Ni) catalyst on the dehydrogenation and rehydrogenation behavior of ball milled lithium alanate ($LiAlH_4$)

R.A. Varin*, L. Zbroniec

Department of Mechanical and Mechatronics Engineering, University of Waterloo, Waterloo, Ontario, Canada N2L 3G1

ARTICLE INFO

Article history:
Received 21 June 2010
Accepted 14 July 2010
Available online 21 July 2010

Keywords:
Solid state hydrogen storage
Hydrogen storage materials
Desorption temperature and kinetics
Lithium alanate ($LiAlH_4$)
Nanometric nickel additive
Ball milling
X-ray diffraction (XRD)
Differential Scanning Calorimetry (DSC)

ABSTRACT

A comprehensive study of the effects of nanometric Ni (n-Ni) additive having a specific surface area (SSA) of 9.5 and 14.5 m^2/g on the dehydrogenation and rehydrogenation behavior of mechanically (ball) milled $LiAlH_4$ has been carried out using Differential Scanning Calorimetry (DSC), X-ray diffraction (XRD) and volumetric hydrogen desorption in a Sieverts-type apparatus under 0.1 MPa H_2 pressure. The $LiAlH_4$ + 1, 5 and 10 wt.% n-Ni mixtures were processed by a simple mixing as well as low energy and high energy mechanical (ball) milling in a unique magneto-mill. No decomposition during milling up to 1 h has been observed for $LiAlH_4$ + 5 and 10 wt.% n-Ni. A mixing of $LiAlH_4$ + n-Ni still results in the melting of $LiAlH_4$. In contrast, doping with 5 and 10 wt.% n-Ni combined with high energy ball milling completely eliminates melting of $LiAlH_4$. Volumetric dehydrogenation studies show that throughout the entire temperature range from 100 °C to 250 °C a $LiAlH_4$ + n-Ni nanocomposite system ball milled under high energy mode always desorbs hydrogen in a solid state without any melting in two stages I and II. Stage I is related to the transformation of $LiAlH_4$ into ($Li_3AlH_6 + Al + H_2$) and Stage II is related to the transformation of Li_3AlH_6 into ($LiH + Al + H_2$). The apparent activation energy of Stage I and II equals ~70 and ~100 kJ/mol, respectively. This can be compared with the apparent activation energy of ball milled undoped $LiAlH_4$ equal to about 90 kJ/mol for both Stage I and II as reported in Ref. [9]. It is also shown that n-Ni is a very potent catalyst destabilizing a ball milled mixture of $LiAlH_4$ + 5 wt.% to the extent that it is capable to desorb slowly quite substantial quantities of hydrogen at RT, 40 and 80 °C. The rate of H_2 release during storage at this temperature range can be easily regulated by increasing or decreasing temperature. These virtues make the $LiAlH_4$ + 5 wt.% n-Ni mixture a potential hydrogen storage material for applications where a continuous supply of hydrogen is required for a prolonged service time as, for example, in some chemical processes where the presence of a reducing atmosphere is required. Rehydrogenation attempts of ball milled dehydrogenated $LiAlH_4$ + 5 wt.% n-Ni have been made. The dehydrogenation temperatures were selected in such a manner as to rehydrogenate either starting from the ($Li_3AlH_3 + Al$) (dehydrogenation at 120 °C) or from the ($LiH + Al$) (dehydrogenation at 170 and 250 °C) phase composition. Rehydrogenation temperatures and pressures of H_2 were in the range of 55–250 °C and 0.2–10 MPa, respectively. Unfortunately, no successful rehydrogenation has been observed under these conditions.

1. Introduction

In the future hydrogen economy a viable solid state hydrogen storage system is needed for efficient supply of pure hydrogen to fuel cells in automotive and non-automotive applications like, for example, portable electronic consumer goods. For a proton exchange membrane (PEM) fuel cell a viable hydrogen storage system requires operating temperature range of approximately 20–100 °C and a practical hydrogen capacity exceeding at least 6 wt.%, particularly, in automotive applications [1]. One of the most interesting hydrides for a solid state hydrogen storage is a complex metal hydride $LiAlH_4$ (lithium alanate) since it can liberate a pretty large theoretical quantity of 7.9 wt.% H_2 below 250 °C [1]. Some metal halides such as $AlCl_3$, $NiCl_2$, $TiCl_3$, $TiCl_3{\cdot}1/3AlCl_3$, $TiCl_4$, VCl_3, $ZrCl_4$, $ZnCl_2$ and VBr_3 were added to $LiAlH_4$ as catalysts that enhanced quite dramatically the kinetics of desorption and in effect lowered the desorption temperature of $LiAlH_4$ [2] (also see Ref. [1] for a more thorough review of pertinent works). Metal fluorides such as TiF_3 [3,4] and NbF_5 [5] were also tried as catalysts for $LiAlH_4$. However, metal halides and fluorides are not the most ideal catalysts since they may locally react with $LiAlH_4$ and form metal salts

* Corresponding author. Tel.: +1 519 888 4567; fax: +1 519 885 5862.
E-mail addresses: ravarin@uwaterloo.ca, ravarin@mecheng1.uwaterloo.ca (R.A. Varin).

0925-8388/$ – see front matter © 2010 Elsevier B.V. All rights reserved.
doi:10.1016/j.jallcom.2010.07.119

Table 1
Characterization of n-Ni produced by Vale Inco Ltd. which was used in this study as an additive.

Sample	Specific surface area (SSA) (m^2/g)	C (wt.%)	O (wt.%)	Shape
n-Ni	9.5	0.46	0.11	Spherical
n-Ni	14.5	0.34	2.46	Filamentary

and free elemental metals or intermetallic compounds of nanometric sizes which most likely act as effective catalysts [1]. A by-product of a metal salt constitutes unnecessary ballast (dead-weight) for the microstructure and reduces the total available hydrogen capacity.

The addition of metallic and especially nanometric size metal catalysts to $LiAlH_4$ has not been investigated so extensively. Balema et al. [6] reported that the elemental Fe as a catalytic additive was much less effective than $TiCl_4$, Al_3Ti, $Al_{22}Fe_3Ti_8$ and Al_3Fe. Resan et al. [7] concluded that the addition of elemental Ti, Fe and Ni did not cause the decomposition of $LiAlH_4$ during ball milling as did metal chlorides. Most recently, Kojima et al. [8], besides metal chlorides and intermetallics, also added nanometric Ni as a catalyst to $LiAlH_4$. They found that the n-Ni doped $LiAlH_4$ decomposed during milling. However, in none of these studies on the effects of elemental metals on $LiAlH_4$ combined techniques such as Differential Scanning Calorimetry (DSC), volumetric desorption and X-ray diffraction (XRD) have ever been used for a quantitative characterization of desorption properties.

The present paper is a companion paper to the most recent one [9] in which we have reported a comprehensive study of the decomposition behavior of both as-received and mechanically (ball) milled undoped $LiAlH_4$ powder (Alfa Aesar) with an initial average particle size of 9.9 ± 5.2 μm. In the present work we report the results of the studies on the very strong catalytic effect of nanometric nickel (n-Ni) produced by Vale Inco Ltd. (Ontario, Canada) on the desorption behavior of the same $LiAlH_4$ powder as investigated in Ref. [9]. The nanocomposites of $LiAlH_4$ doped with n-Ni were processed by controlled ball milling in the magneto-mill Uni-Ball-Mill 5 and subsequently investigated by Differential Scanning Calorimetry (DSC), X-ray diffraction (XRD) and volumetric hydrogen desorption in a Sieverts-type apparatus. The results obtained in the present work are compared to the results reported in Ref. [9] and the differences in the behavior arising due to the catalytic action of n-Ni are discussed in view of the microstructural evolution as observed by XRD. After dehydrogenation some rehydrogenation attempts have been also made that are discussed.

2. Experimental

As-received $LiAlH_4$ (97% purity) from Alfa Aesar and specialty nanometric Ni (n-Ni) produced as experimental batches by Vale Inco Ltd., Mississauga, Ontario [10], were mixed to $LiAlH_4$ + 1, 5 and 10 wt.% n-Ni composition. The chemical composition and morphological characterization of the nanometric Ni used in the present work are given in Table 1. The specific surface area (SSA) was measured by the BET method in the Vale Inco Ltd.'s laboratories. We have found no measurable difference in the catalytic effect of 9.5 and 14.5 m^2/g nanonickels and as such, they will be referred to as "n-Ni" further in the manuscript without any reference to their SSA.

Controlled mechanical milling (CMM) was carried out for 15 min in high purity hydrogen gas atmosphere (purity 99.999%: O_2 <2 ppm; H_2O <3 ppm; CO_2 <1 ppm; N_2 <6 ppm; CO <1 ppm; THC <1 ppm) under ~600 kPa pressure in the magneto-mill Uni-Ball-Mill 5 manufactured by A.O.C. Scientific Engineering Pty Ltd., Australia [1,11–13]. In this particular ball mill the varying energy milling modes can be achieved by using one or two strong NdFeB magnets and changing their angular positions and the number of hard steel balls (25 mm in diameter each) in a milling vial. Fig. 1 shows a set up for a strong impact mode IMP68 with two magnets positioned at 6 and 8 o'clock, at the distance of 10 and 2 mm, respectively, from the milling vial (working distance – WD) and 4 hard steel balls in the vial. A modification of IMP68 mode is IMP69 where the magnets are positioned at 6 and 9 o'clock. The ball-to-powder weight ratio (R) used in this work was either ~40 (R40) or 132 (R132). We found no measurable difference between these two R's and eventually we set up at R132 as it saves the quantity of powder used. The rotational speed of milling vial was ~200 rpm. After loading with powder, an air-tight milling vial with

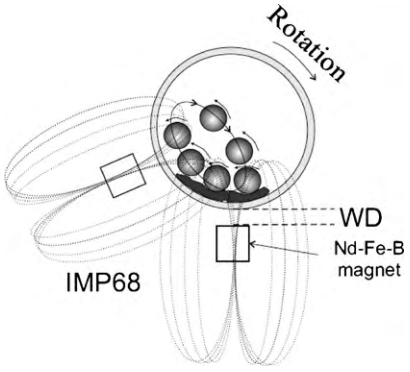

Fig. 1. A schematic of the cross-section of the milling vial and the approximate trajectories of the ball movement under IMP68 mode of milling in the magneto-mill Uni-Ball-Mill 5.

an O-ring, equipped with a pressure valve mounted in the lid (Fig. 1), was always evacuated and purged several times with high purity argon (Ar) gas (99.999% purity) before final pressurization with H_2. All the powder handlings after milling were performed in a purged glove box under overpressure of high purity argon.

The crystalline structure of powders was characterized by Bruker D8 diffractometer using a monochromated CuKα_1 radiation (λ = 0.15406 nm) produced at an accelerating voltage of 40 kV and a current of 30 mA. The scan range was from 2θ = 10–90° and the scan rate was 3° min^{-1}. Powder was loaded in a glove box filled with Ar into a home-made environmental brass holder with a Cu plate for powder support. A few XRD tests were made on a plastic support which gave a characteristic broad peak at 2θ < 20° and was eventually discarded. Upper and lower part of the environmental holder is sealed through a soft-rubber O-ring and tightened using threaded steel bolts with nuts.

The nanograin (crystallite) size of phases residing in the milled powders was calculated from the broadening of their respective XRD peaks. Since the Bragg peak broadening in an XRD pattern is due to a combination of grain refinement (nanograin/crystallite) and lattice strains, it is customary to use computing techniques by means of which one can separate these two contributions. The separation of crystallite size and strain was obtained from Cauchy/Gaussian approximation by the linear regression plot according to the following equation [14]:

$$\frac{\delta^2(2\theta)}{\tan^2\theta} = \frac{K\lambda}{L}\left(\frac{\delta(2\theta)}{\tan\theta\,\sin\theta}\right) + 16e^2 \quad (1)$$

where the term $K\lambda/L$ is the slope, the parameter L is the mean dimension of the nanograin (crystallite) composing the powder particle, K is constant (~1) and e is the so-called "maximum" microstrain (calculated from the intercept), λ is the wave length and θ is the position of the analyzed peak maximum. The term $\delta(2\theta) = B[1 - (b^2/B^2)]$(rad) is the instrumental broadening-corrected "pure" XRD peak profile breadth [14] where B and b are the breadths in radians of the same Bragg peak from the XRD scans of the experimental and reference powder, respectively. They were calculated by the software Traces™ v. 6.5.1 as the full-widths at half maximum, FWHM, after background removal. A compound LaB_6, the National Institute of Standards and Technology (NIST) standard reference material (SRM) 660 was used as a reference for subtracting the instrumental broadening from FWHM. It must be noted that when the FWHM of the instrumental line profiles were obtained in this manner, the Bragg peaks for the LaB_6 SRM were at different 2θ angles than those of the analyzed phases in the milled powders. The interpolated FWHM values between angles for the SRM peaks were found using a calibration curve.

The hydrogen desorption was evaluated using a second generation volumetric Sieverts-type apparatus custom-built by A.O.C. Scientific Engineering Pty Ltd., Australia. This apparatus built entirely of austenitic stainless steel allows loading of a powder sample in a glove box under argon and its subsequent transfer to the main unit in a sealed austenitic stainless steel sample reactor without any exposure to the environment. The weight of the powder sample in the desorption experiments was in the range of 20–30 mg. The calibrated accuracy of desorbed hydrogen capacity is about ±0.1 wt.% H_2 and that of temperature reading ±0.1 °C. Before starting the desorption test, the inner tubing of the apparatus and reactor were evacuated and purged 4 times with argon and then two times with hydrogen. The furnace of the apparatus was heated separately to the desired test temperature and subsequently inserted onto a tightly sealed powder sample reactor inside which an atmospheric pressure of 0.1 MPa H_2 was kept. Hence, the beginning of the desorption test was in reality pseudo-isothermal before the powder sample temperature reached the desired value. However, the calibrated time interval within which the powder sample in the reactor reaches the furnace temperature is ~400–600 s in the 100–350 °C range, which is negligible compared to the desorption completion time especially at temperatures below 200 °C. Therefore, one can consider the test as being "isothermal" for any practical purposes at this range of temperatures. The amount of desorbed hydrogen was calculated from the ideal gas law as described in

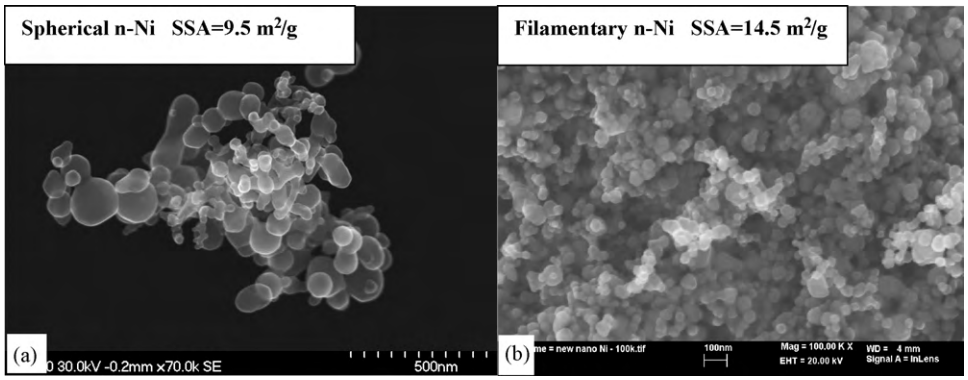

Fig. 2. Scanning electron micrographs of the morphology of Vale Inco Ltd. nanometric Ni (n-Ni) with (a) SSA = 9.5 m^2/g and (b) SSA = 14.5 m^2/g used in this work.

detail in Ref. [1]. Hydrogen desorption curves were also corrected for the hydrogen gas expansion due to the increase in temperature.

Rehydrogenation attempts were conducted immediately after a powder was desorbed without removing it from a sealed reactor by simply admitting H_2 under desired pressure and increasing/decreasing temperature to a desired level.

The apparent activation energy for desorption process was estimated from the obtained volumetric desorption curves at corresponding temperatures using the Arrhenius plot of k values with temperature [1]:

$$k = k_o e^{-E_A/RT} \quad (2)$$

where E_A is the activation energy, R is the gas constant and T is the temperature. The rate constant k was determined using the Johnson–Mehl–Avrami–Kolmogorov (JMAK) equation [1]:

$$\alpha = 1 - e^{-(kt)^\eta} \quad (3)$$

where η is the reaction exponent (the Avrami exponent) related to the transformation mechanism, taken as a free value characteristic for each individual temperature [1,15] rather than a fixed value for all temperatures, and α is the desorption fraction at time t.

The thermal behaviour of powders was studied by Differential Scanning Calorimetry (DSC) (Netzsch 404) of ~6 mg powder sample with heating rate of 10 °C/min and argon flow rate of 100 ml/min. The powder was transported to a DSC instrument in a glass vial filled with Ar and then quickly loaded into an Al_2O_3 crucible with a lid. This operation took about 2–3 min and only for that short period of time the powder could be in contact with air.

Finally, it must be pointed out that all the tests described in the following sections were carried out within a couple of days from the completion of ball milling of powders in order to avoid any long-term storage degradation effects [1].

3. Results and discussion

3.1. Microstructure of nanometric Ni (n-Ni) and $LiAlH_4$ + n-Ni powder mixtures after milling

SEM micrograph of as-received $LiAlH_4$ which was processed with n-Ni before compositing was already shown in Ref. [9] and will not be repeated here. Fig. 2 shows scanning electron micrographs (SEM) of the two varieties of nanometric Ni powder used as a catalyst in the present work. SEM observations of the milled and n-Ni doped $LiAlH_4$ powder showed that the n-Ni particles were uniformly dispersed within the $LiAlH_4$ particles and on their surfaces (micrographs not shown here as they are trivial). The average final particle size after ball milling was on the order of ~3 μm which is very similar to the one obtained after milling of undoped $LiAlH_4$ [9].

Fig. 3 shows two XRD patterns of n-Ni doped $LiAlH_4$ after milling as compared to the XRD of $LiAlH_4$ after milling under the same milling conditions. It is clearly seen that all three XRD patterns are nearly identical showing that the predominant phase in the microstructure of all three powders is $LiAlH_4$ with small amount of impurities such as lithium hydroxide hydrate ($LiOH–H_2O$) and elemental Al which were also reported for undoped $LiAlH_4$ [9]. Within the resolving capability of XRD technique there is no evidence of the existence of Li_3AlH_6 after a high energy ball milling of undoped $LiAlH_4$ or the one doped with 5 wt.% n-Ni. In a few more milling tests we increased the amount of n-Ni doping to 10 wt.% and extended the milling time to 1 h with the same result, i.e. no evidence of the presence of Li_3AlH_6 in an XRD pattern. Therefore, it is clear that $LiAlH_4$ doped with 5 or 10 wt.% n-Ni does not decompose to a detectable degree during milling up to at least 1 h duration under high energy impact mode. At this moment, the reader must recall that Kojima et al. [8] reported that the $LiAlH_4$ doped with 5 wt.% of n-Ni partially decomposed during ball milling for 24 h at room temperature. In the present work we did not extend milling time for over 1 h as it is unnecessary from the technological point of view and therefore, we cannot speculate whether or not much prolonged milling time would eventually lead to a partial decomposition of $LiAlH_4$ + 5 or 10 wt.% n-Ni.

Grain size estimate of $LiAlH_4$ from the peak breadths of Bragg peaks in XRD patterns in Fig. 3 using Eq. (1) shows that the average grain/crystallite size of $LiAlH_4$ + 5 or 10 wt.% n-Ni powders, ball milled under high energy IMP68 mode, is close to ~80 nm with an excellent coefficient of fit R^2 equal to 0.96–0.98. This is a very similar grain size range to the one reported for ball milled undoped $LiAlH_4$ in Ref. [9].

3.2. Thermal decomposition and microstructural evolution during DSC tests

Fig. 4b–f shows the evolution of DSC curves with increasing ball milling energy for the $LiAlH_4$ + 5 wt.% n-Ni nanocomposite as compared to the behavior of undoped $LiAlH_4$ ball milled under high energy mode in Fig. 4a. According to the discussion in Ref. [9] the first exothermic peak at 143.8 °C is most likely due to the reaction of the surface aluminum-hydroxyl groups owing to the presence of impurities as first reported by Block and Gray [16] and the endothermic peak at 174.4 °C is due to the melting of $LiAlH_4$. As reported in Ref. [9] a deep exothermic peak at 201.1 °C is a superposition of three events: the decomposition of molten $LiAlH_4$ into (Li_3AlH_6 + Al + H_2), initial decomposition of Li_3AlH_6 into (LiH + Al + H_2) and solidification of Li_3AlH_6. Finally, a small and broad endothermic peak at 234.7 °C is due to the final decomposition of the small amount of remaining Li_3AlH_6. The last peak at over 400 °C is usually ascribed to the decomposition of LiH which was formed as a result of decomposition of Li_3AlH_6. However, decomposition of LiH has no practical value since its temperature is too high.

Fig. 4b shows that the addition of n-Ni to $LiAlH_4$ by simple mixing without ball milling does not change the reference DSC scan in Fig. 4a. In contrast, even relatively low energy ball milling of n-Ni doped $LiAlH_4$ using 1 weak magnet and 2 balls changes profoundly a DSC scan as shown in Fig. 4c. Both melting peak of $LiAlH_4$ (at 168 °C) and the following exo peak at 169 °C become very small. As

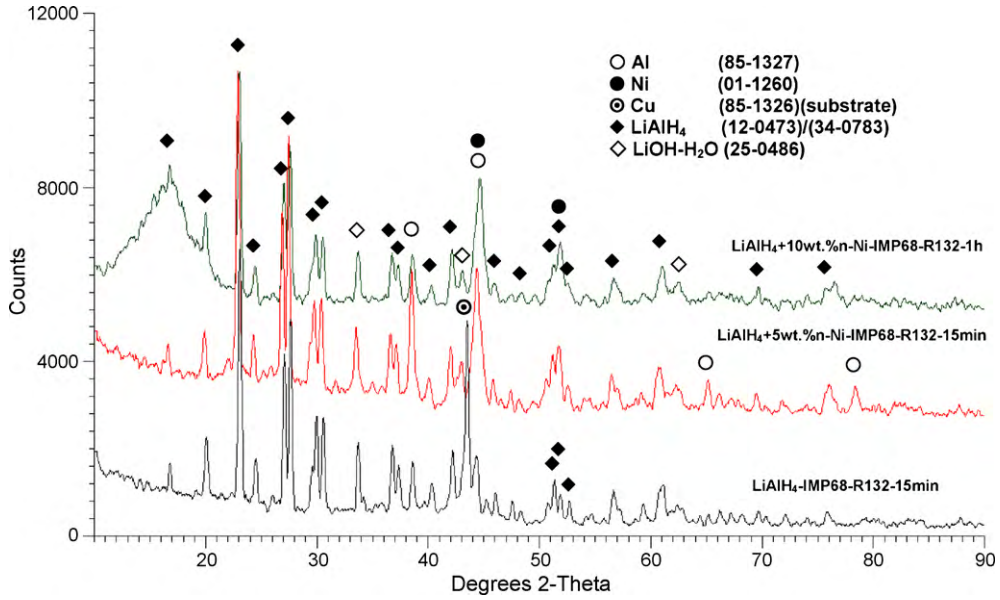

Fig. 3. XRD patterns of ball milled $LiAlH_4$ + 5 wt.% n-Ni powder compared with the XRD pattern of ball milled undoped $LiAlH_4$. JCPDS file numbers for phase identification are given in parenthesis. A broad peak at $2\theta < 20^\circ$ arises from a plastic holder support which was eventually discarded.

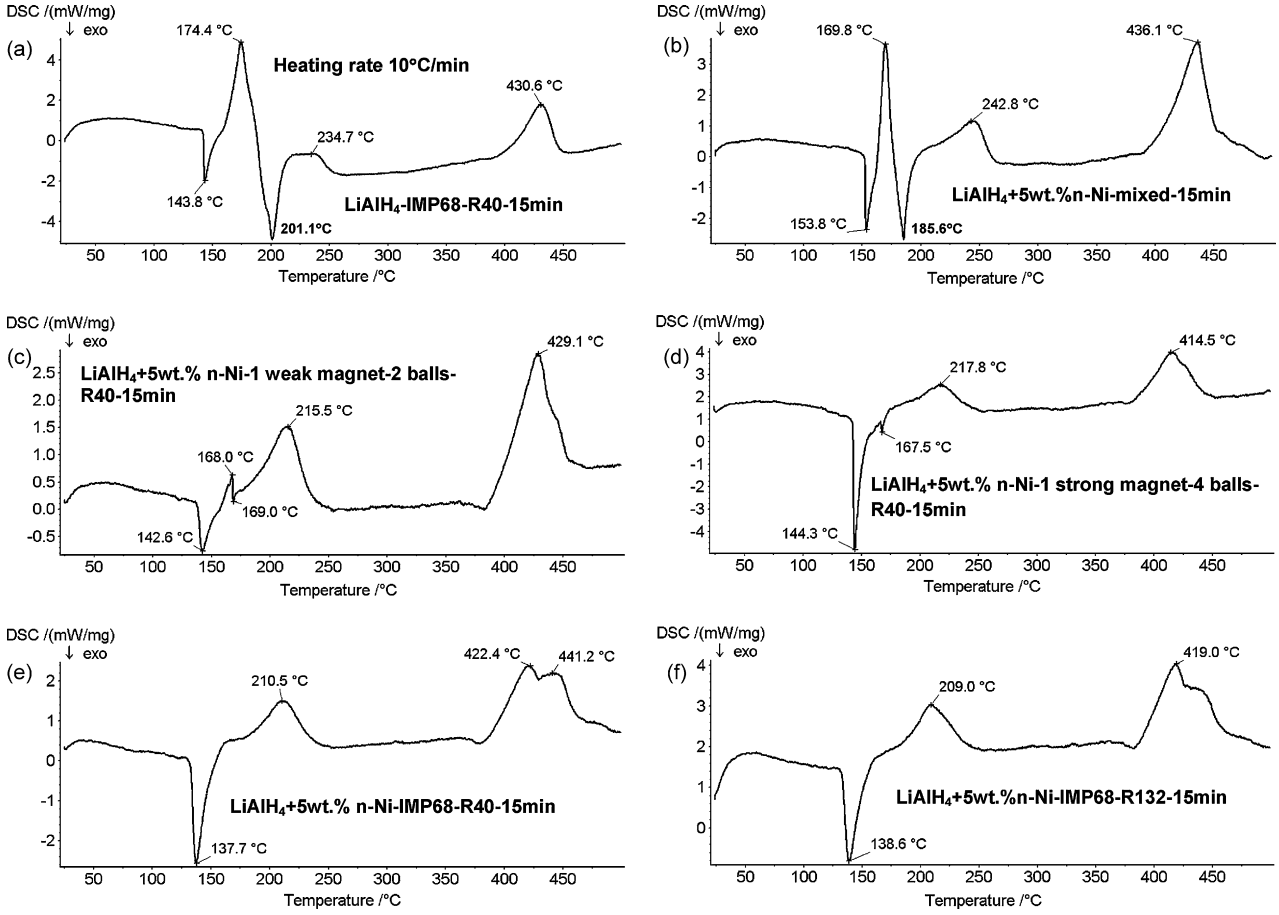

Fig. 4. DSC curves for $LiAlH_4$ and $LiAlH_4$ + 5 wt.% n-Ni ball milled under varying energy milling modes. (a) $LiAlH_4$ milled for 15 min under IMP68 mode, R40. (b) $LiAlH_4$ + 5 wt.% n-Ni mixed for 15 min. (c) $LiAlH_4$ + 5 wt.% n-Ni milled for 15 min under low energy shearing mode with 1 weak magnet, 2 balls and R40. (d) $LiAlH_4$ + 5 wt.% n-Ni milled for 15 min using 1 strong magnet, 4 balls, R40. (e) $LiAlH_4$ + 5 wt.% n-Ni milled for 15 min under high energy milling mode IMP68 and R40. (f) $LiAlH_4$ + 5 wt.% n-Ni milled for 15 min under high energy milling mode IMP68, R132. Heating rate was 10 °C/min.

can be seen in Fig. 4d more energetic milling using 1 strong magnet and 4 balls completely eliminates melting peak of $LiAlH_4$ while only a very small exothermic peak is visible at 167.5 °C. High energy ball milling of n-Ni doped $LiAlH_4$ using IMP68 mode with R40 or 132 completely eliminates the endothermic melting peak of $LiAlH_4$ and only one endothermic peak around 210 °C is seen in Fig. 4e

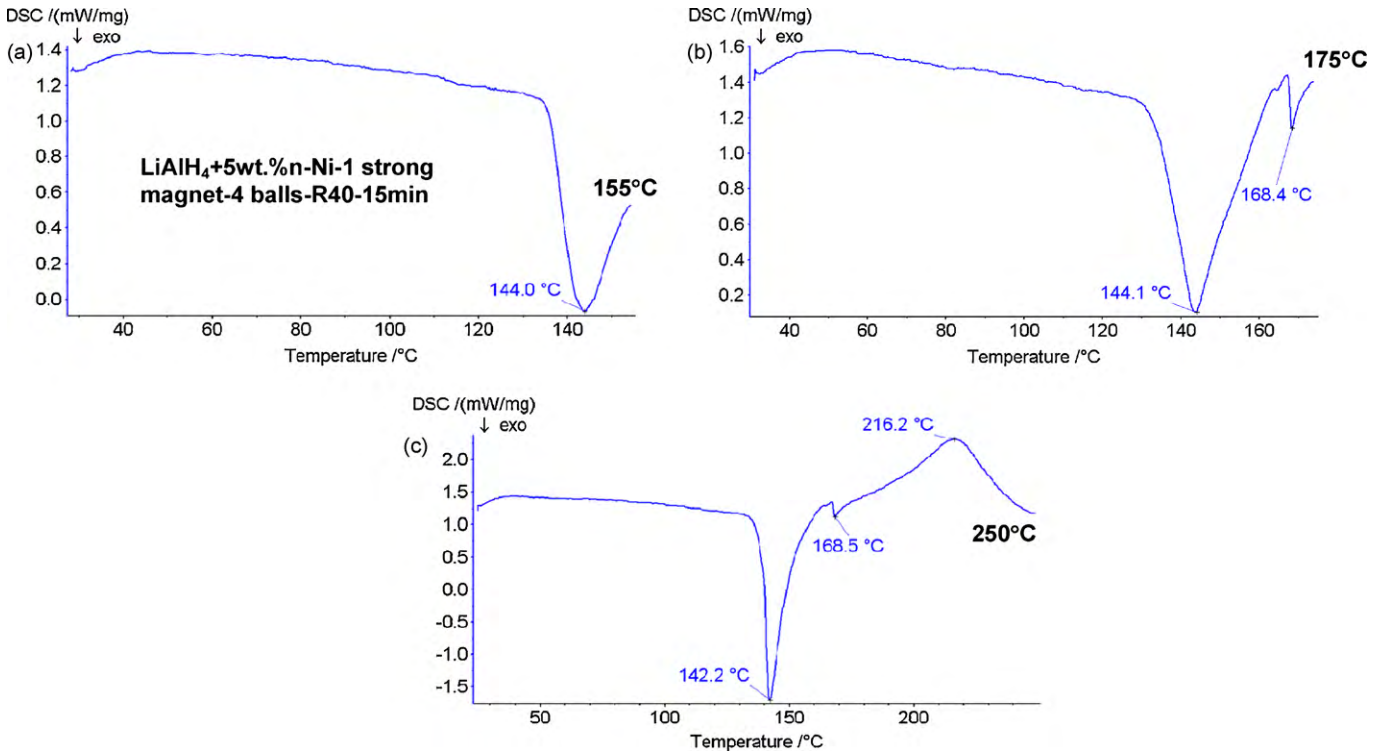

Fig. 5. Isothermal sectioning of DSC test for the $LiAlH_4$ + 5 wt.% n-Ni powder ball milled for 15 min under low energy shearing (LES) mode with one strong magnet, 4 balls and R40. A DSC test was stopped at (a) 155 °C, (b) 175 °C, and (c) 250 °C. Heating rate was 10 °C/min.

and f. However, a strong exothermic peak is visible in Fig. 4e and f whose peak temperature is shifted below 140 °C. This sequence of the effect of milling energy on thermal behavior clearly shows that the n-Ni catalyst must be very intimately embedded in the $LiAlH_4$ particles in order to be able to exert a strong catalytic action on the alanate matrix. Apparently, as shown by the experiment with a simple mixing (Fig. 4b) it is insufficient that the n-Ni particles are distributed solely on the surface of particles due to mixing but they must be also embedded in the bulk of the particles which is only achieved by high energy ball milling under IMP68/69.

In order to shed more light on the nature of the above reactions occurring in the nanocomposite a low energy shearing (LES) ball milled $LiAlH_4$ + 5 wt.% n-Ni mixture was subjected to a thermal sectioning in DSC at pre-determined temperatures following the procedure outlined in Ref. [9]. As shown in Fig. 5a–c each DSC heating test was stopped at a temperature of 155, 175 and 250 °C, respectively. After stopping the test the powder sample from a crucible was immediately taken for an XRD test. The corresponding XRD patterns are shown in Fig. 6.

The microstructure of powder stopped at 155 °C, just beyond the peak temperature of the first exothermic peak (Fig. 5a), consists of Li_3AlH_6, Al and obviously Ni (n-Ni). This clearly indicates that up to 155 °C, the $LiAlH_4$ phase was nearly completely decomposed in a solid state according to the following apparent exothermic reaction with a maximum at 144 °C (Fig. 5a):

$$LiAlH_4\,(solid) \rightarrow 1/3Li_3AlH_6\,(solid) + 2/3Al\,(solid) + H_2 \qquad (4)$$

As reported in Ref. [9] for undoped $LiAlH_4$ the above reaction starts occurring immediately after $LiAlH_4$ melts. In the present case, due to the fact that the melting of $LiAlH_4$ is nearly completely eliminated for this powder (Fig. 4d), $LiAlH_4$ simply starts decomposing without melting at a much lower temperature range as a result of an enormous acceleration of decomposition process by doping with a n-Ni catalytic additive. It is interesting to point out that reaction (4) occurs in the same temperature range in Figs. 4d–f and 5a as the first observed exothermic reaction assigned to the surface aluminum-hydroxyl groups which occurs in undoped $LiAlH_4$ [9] and can also be clearly seen in Fig. 4a and b. At this moment, it is unclear if this is just a coincidence or indeed, the reaction of the surface aluminum-hydroxyl groups triggers a spontaneous decomposition of ball milled n-Ni doped $LiAlH_4$ at temperatures much lower than its melting point. Furthermore, it is not clear if the origin of the exothermic nature of the first peak in Figs. 4d–f and 5 is related to the inherent exothermic nature of the surface aluminum-hydroxyl groups reaction or indeed, reaction (4) is simply exothermic in its nature despite the fact that melting has been eliminated. This problem needs more studies. It must, however, be pointed out that the exothermic peaks assigned to the decomposition of $LiAlH_4$ in a solid state have also been reported for $LiAlH_4$ ball milled with TiF_3 [4] and NbF_5 [5] catalytic additives. Hence, it seems that regardless of the type of catalyst an exothermic event is always associated with the decomposition of $LiAlH_4$ in a solid state according to reaction (4).

A very small exothermic peak is still recognizable in Fig. 4d at 167.5 °C and Fig. 5b at 168.4 °C. Most likely, this peak is related to the decomposition of the remaining amount of $LiAlH_4$ which was not in an intimate contact with a n-Ni catalyst due to lower milling energy (LES with 1 magnet only) than IMP68/69 and resulting inhomogeneous re-distribution of n-Ni. One should notice that this peak disappears after high energy ball milling when n-Ni becomes completely homogeneously re-distributed within the bulk and at the surfaces of powder particles. As shown in the XRD pattern in Fig. 6, the microstructure of powder stopped at 175 °C (Fig. 5b), just beyond the small remaining exothermic peak, still consists of Li_3AlH_6, Al and Ni (n-Ni) with a small amount of LiOH (note a very weak peak (1 0 1) 100% intensity at $2\theta = 32.8°$, JCPDS 04-0708). The presence of a small quantity of LiOH may indicate that around this temperature Li_3AlH_6 starts gradually decomposing according to the well-known endothermic reaction in a solid state [1,9]:

$$1/3Li_3AlH_6\,(solid) \rightarrow LiH(solid) + 1/3Al\,(solid) + 0.5H_2 \qquad (5)$$

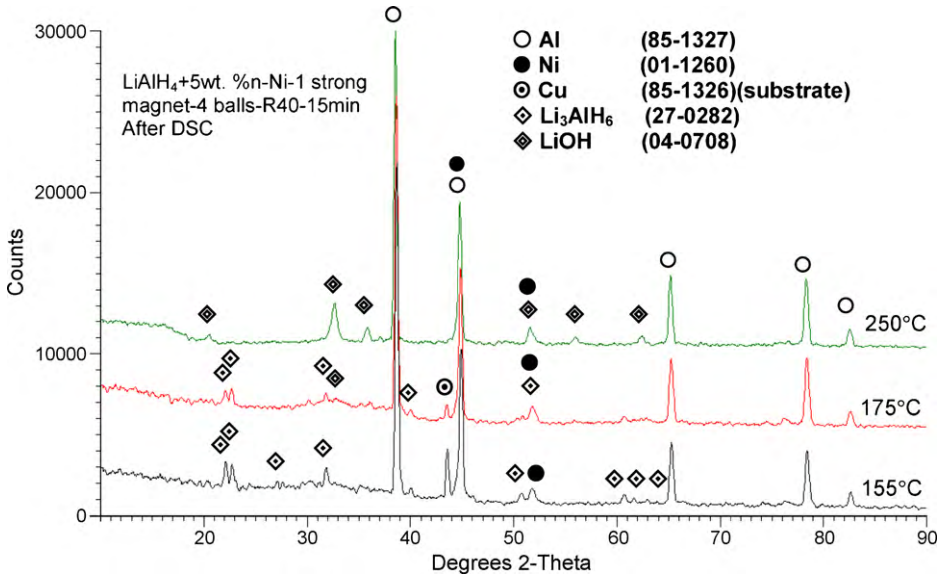

Fig. 6. XRD patterns taken from the powder sample obtained in a DSC thermal sectioning test up to 155, 175, and 250 °C. JCPDS file numbers for phase identification are given in parenthesis.

As discussed in Ref. [9] the resulting LiH hydride could have been hydrolyzed into LiOH. There are a few possibilities here. First is that LiH hydrolyzed during transfer of powder from a vial to the DSC chamber. Second possible mechanism is that since our DSC system works under a constant argon gas flow in an essentially open configuration (as most of them do) some air might have penetrated into a chamber. Third, some minutiae air leakage might have occurred into the environmental XRD holder used in the present work whose soft-rubber O-ring could be, on occasions, contaminated with a few embedded powder particles during loading in a glove box and as such it was not fully tight after assembly. Similar behavior is seen in Fig. 6 for the XRD pattern of the powder stopped at 250 °C. It shows besides Ni (n-Ni) also strong diffraction peaks of Al and LiOH. The temperature of 250 °C is just beyond the endothermic peak of reaction (5) with the maximum at 216.2 °C in Fig. 5c. That requires that according to reaction (5) the microstructure should consists of Al and some quantity of LiH. However, a fraction of the latter was apparently converted into LiOH as discussed above.

3.3. Volumetric desorption behavior at elevated temperatures, apparent activation energy for hydrogen desorption and corresponding microstructural evolution

In this section we will discuss a volumetric desorption behavior at 100 °C and higher temperatures.

Fig. 7 shows the effect of n-Ni content and milling time for 15 min and 1 h on the desorption curves at 100 °C under 0.1 MPa H_2 pressure. At this temperature, $LiAlH_4$ + 1 wt.% n-Ni ball milled for

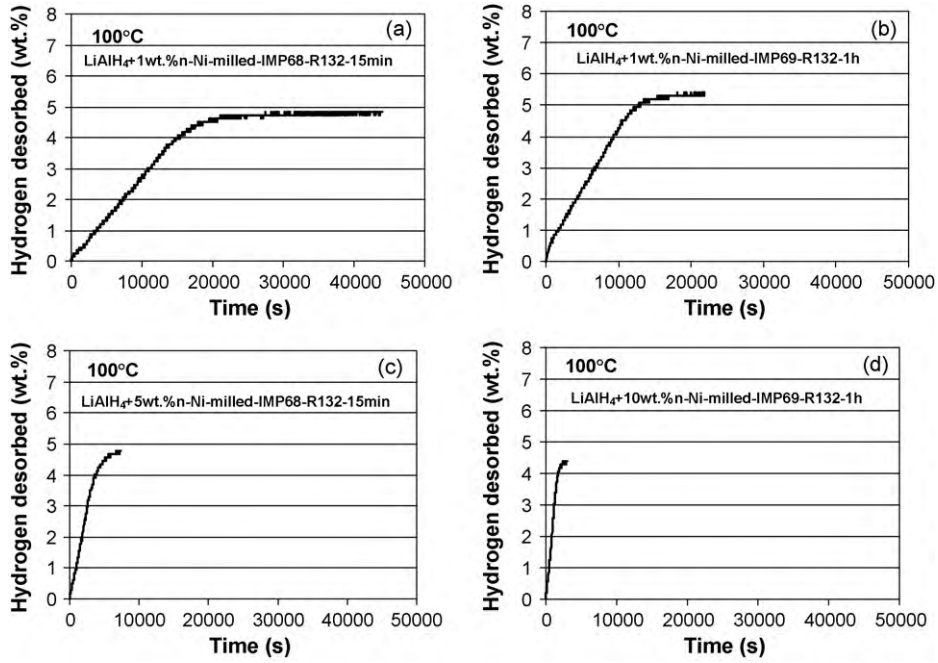

Fig. 7. Volumetric desorption curves at 100 °C under 0.1 MPa H_2 pressure for the ball milled $LiAlH_4$ + 1, 5 and 10 wt.% n-Ni system with R132. (a) 1 wt.% n-Ni, IMP68, 15 min milling. (b) 1 wt.% n-N, IMP69, 1 h milling. (c) 5 wt.% n-Ni, IMP68, 15 min milling. (d) 10 wt.% n-Ni, IMP69, 1 h milling.

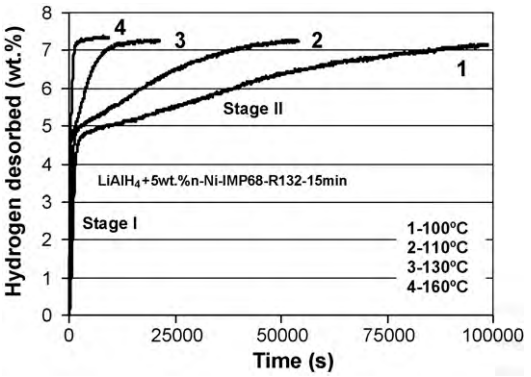

Fig. 8. Volumetric desorption curves at various temperatures under 0.1 MPa H_2 pressure (atmospheric) for the ball milled $LiAlH_4$ + 5 wt.% n-Ni system which were used for the apparent activation energy estimation.

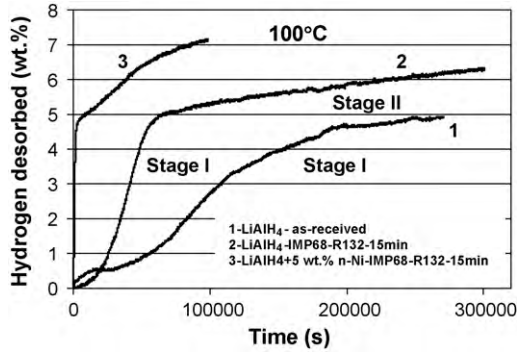

Fig. 9. Comparison of volumetric desorption curves at 100 °C under 0.1 MPa H_2 pressure for as-received undoped $LiAlH_4$ (curve 1), ball milled undoped $LiAlH_4$ (curve 2) and ball milled $LiAlH_4$ + 5 wt.% n-Ni (curve 3).

15 min is able to desorb about 5 wt.% H_2 within ~30,000 s (Fig. 7a). Increasing of milling time to 1 h reduces desorption time by about half (~15,000 s) (Fig. 7b). However, an increase of the n-Ni catalytic additive to 5 wt.% allows desorption of 5 wt.% H_2 within ~10,000 s after ball milling for only 15 min (Fig. 7c). Increasing the amount of catalytic n-Ni dopant to 10 wt.% and milling time to 1 h does not improve the kinetics of desorption in any measurable way. Therefore, it seems that the 5 wt.% content of n-Ni catalyst and 15 min milling duration is the most optimal combination to achieve an enormous improvement of desorption kinetics of $LiAlH_4$.

Fig. 8 shows desorption curves for the optimal combination of $LiAlH_4$ + 5 wt.% n-Ni and the milling duration of 15 min. All desorption curves clearly exhibit a two-stage desorption process as designated by Stage I and II. That means that decomposition process involves reactions (4) and (5). Also, it is clearly seen that allowing a longer desorption time at 100 °C the ball milled $LiAlH_4$ + 5 wt.% n-Ni system is able to desorb ~7.1 wt.%H_2 within ~98,000 s under atmospheric pressure of H_2. To the best of our knowledge there is no other complex metal hydride at present that would desorb this amount of H_2 at such a low temperature under atmospheric pressure of H_2. Fig. 9 shows a comparison of a desorption curve at 100 °C for $LiAlH_4$ + 5 wt.% n-Ni with those for as-received and ball milled undoped $LiAlH_4$. It is clearly seen that the desorption kinetics for as-received $LiAlH_4$ are the slowest ones resulting in desorption of ~5 wt.% H_2 after ~270,000 s. Within this time period desorption occurs only in Stage I (reaction (4)). Ball milling of $LiAlH_4$ increases kinetics such that about 6.3 wt.% H_2 is desorbed within ~300,000 s in Stage I and partially II (reactions (4) and (5)). As shown above, the addition of 5 wt.% n-Ni accelerates desorption to the extent that the quantity of ~5.0 wt.%H_2 is desorbed within ~12,000 s and ~7.1 wt.%H_2 is desorbed within ~98,000 s.

For the calculations of the apparent activation energy of desorption the free reaction exponent η for each temperature [1,15] and the corresponding rate constant k in Eq. (3) were calculated from a linear interpolation of the typical plots $\ln[-\ln(1-\alpha)]$ vs. $\ln t$ [1]. The details of calculations with Eq. (3) are fully explained in Ref. [9] for an interested reader. Fig. 10 shows the Arrhenius plots for the estimate of the apparent activation energy for the ball milled $LiAlH_4$ + 5 wt.% n-Ni mixture in Stage I (Fig. 10a) and II (Fig. 10b) which also show excellent coefficients of fit to Eq. (2) giving a testimony to the accuracy of the method. It can be seen that for Stage I (reaction (4) in a solid state) and Stage II (reaction (5)) the apparent activation energy equals to ~70 and ~100 kJ/mol, respectively. These values can be compared to the apparent activation energy of ball milled undoped $LiAlH_4$ which for Stage I and II is equal to ~92.5 and ~92 kJ/mol, respectively [9]. For another comparison, Andreasen [17] reported that the apparent activation energy of desorption for $LiAlH_4$ doped with 2 mol% $TiCl_3$–1/3$AlCl_3$, as obtained from the Kissinger method [1], was equal to 89 and 103 kJ/mol for Stage I and II, respectively. For pristine $LiAlH_4$ they reported corresponding apparent activation energies equal to 81 and 108 kJ/mol, respectively. It seems that the apparent activation energy for Stage I of ball milled metal chloride doped $LiAlH_4$ in Ref. [17] is even slightly higher than that of pristine $LiAlH_4$ in their work. Blanchard et al. [18] used synchrotron X-ray diffraction method to study Stage I desorption process of $LiAlD_4$ doped with 2 mol% $TiCl_3$–1/3$AlCl_3$ and VCl_3 for which they obtained the apparent activation energy equal to 95 and 90 kJ/mol, respectively. However, in contradiction to the results obtained in this work and those reported in Refs. [17,18], Chen et al. [19] and Hima Kumar et al. [20] reported unusually low apparent activation energies for Stage I desorption for $LiAlH_4$ doped with 2 mol% $TiCl_3$–1/3$AlCl_3$ and 5 wt.% CNF (carbon nanofibers) equal to ~43 and 46 kJ/mol, respectively. These values seem to be unreasonably low and may have resulted from the usage of inappropriate desorption curves obtained at too high temperatures for which Stage I desorption rate was too fast and occurred almost entirely during temperature stabilization interval. In the present work, for the estimate of the apparent activation energy we used only those desorption curves for which majority of desorption in Stage I occurred at an already stabilized constant temperature (pseudo-isothermal condition). More discussion of this subject the reader can find in Ref. [9].

The above comparison very clearly indicates that the n-Ni catalytic additive is indeed a very potent catalyst which substantially reduces the apparent activation of Stage I (reaction (4) in a solid state). The n-Ni catalyst seems to be more effective than metal chlorides. Comparing the apparent activation energies for Stage I for a metal chloride reported in Refs. [17,18] and n-Ni doped $LiAlH_4$ from this work it is clear that n-Ni substantially affects the apparent activation of Stage I while metal chlorides do not. It must be kept in mind that, most likely, metal chlorides react with $LiAlH_4$ forming a salt and a free elemental metal or intermetallic which, in turn, acts as a catalyst [1]. Thus the catalytic action mechanism seems to be similar for a metallic catalytic additive and chloride (in reality its elemental metal) but the former seems to be still more effective.

The above data also show that the rate controlling stage in the entire decomposition process of $LiAlH_4$ through Stage I and II is the decomposition of Li_3AlH_6 which remains sluggish despite the presence of a strong n-Ni catalyst. Similar behavior seems to be confirmed by comparing the apparent activation energies estimated in Refs. [17,18] for pristine and metal chloride doped $LiAlH_4$ as discussed above. It seems that neither a metal chloride nor metallic n-Ni affects measurably the apparent activation energy of Stage II (reaction (5)).

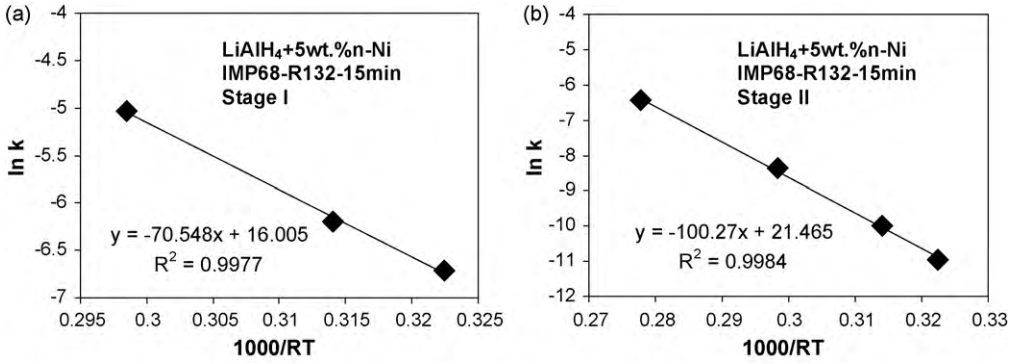

Fig. 10. The Arrhenius plots of rate constant k with temperature for estimation of the apparent activation energy of hydrogen desorption for the ball milled $LiAlH_4$ + 5 wt.% n-Ni system. (a) Stage I at 100, 110 and 130 °C; (b) Stage II at 110, 110, 130 and 160 °C.

In order to investigate the microstructural evolution during decomposition of the ball milled $LiAlH_4$ + 5 wt.% n-Ni mixture at 100 °C as represented by a volumetric desorption curve 1 in Fig. 8, the XRD patterns were acquired from powder desorbed for the time of ~7200 and 98,000 s which corresponds to the end of Stage I (reaction (4)) and Stage II (reaction (5)) at curve 1 in Fig. 8, respectively. These two XRD patterns are compared to the one taken directly after milling in Fig. 11. The pattern of milled $LiAlH_4$ is quite typical as the one shown in Fig. 3 showing the presence of the nanostructured majority phase $LiAlH_4$ and small amounts of impurities Al and LiOH–H_2O, as discussed earlier. The XRD pattern of the powder taken after 7200 s (~5 wt.%H_2 desorbed) at the end of Stage I (reaction (4)) shows that the microstructure consists of Li_3AlH_6 which clearly indicates that the decomposition of the initial nanostructured $LiAlH_4$ is completed. A "shoulder" is observed at the foot of the (2 0 0) Al peak (2θ = 44.70°) which as discussed in Ref. [9] most likely corresponds to the position of a principal 100% intensity (2 0 0) (2θ = 44.35°) peak of LiH. Therefore, it is quite likely that some amount of LiH is present in the microstructure indicating that, indeed, reaction (4) has been completed and reaction (5) begins after 7200 s at 100 °C. At the end of Stage II after ~98,000 s of desorption Fig. 11 shows that there are very strong Al peaks and remnants of Li_3AlH_6 whose very weak intensities confirms that the decomposition process of Li_3AlH_6 according to reaction (5) is near completion. Reaction (5) also requires the presence of LiH in the microstructure and a "shoulder" observed at the foot of the (2 0 0) Al peak (2θ = 44.70°) on this XRD pattern strongly suggests that LiH is, indeed, another phase present.

3.4. Slow desorption at ambient conditions and corresponding microstructural evolution

A striking discovery made in the present work is that the ball milled $LiAlH_4$ + n-Ni system is able to desorb hydrogen at very low temperatures. Observations of slow decomposition of $LiAlD_4$ catalyzed by TiF_3 and VCl_3 have already been reported [3,21] but this phenomenon has never been investigated quantitatively and the effects of n-Ni on slow decomposition have never been reported.

The ball milled powders were stored under Ar in glass vials at room temperature (RT) as well as at 40 and 80 °C in an oven. Subsequently, after a pre-determined time duration samples from each vial were extracted in an argon-filled glove box for a volumetric desorption test at 140 and 170 °C in a Sieverts-type apparatus. Desorption test was carried out until a desorption curve reached near saturation. A typical set of volumetric desorption curves after storing at RT is shown in Fig. 12. It can be clearly seen that the desorbed H_2 capacity gradually decreases with increasing storage

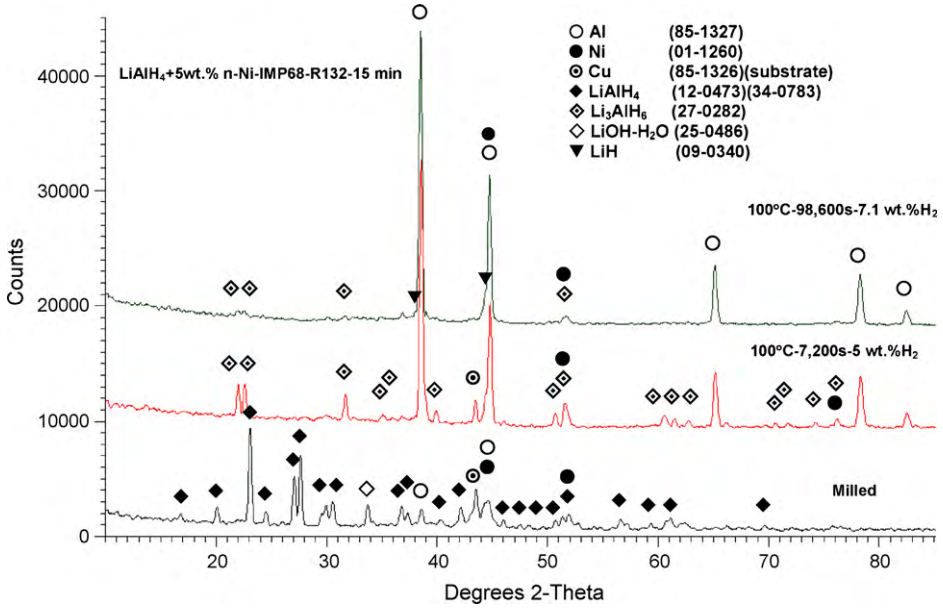

Fig. 11. XRD patterns showing the microstructural evolution during decomposition of the ball milled $LiAlH_4$ + 5 wt.% n-Ni mixture at 100 °C under 0.1 MPa H_2 pressure (volumetric desorption curve 1 in Fig. 8) as compared to the microstructure of the ball milled mixture.

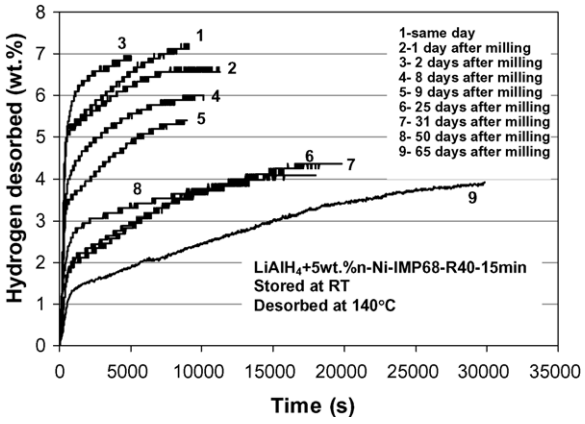

Fig. 12. Volumetric desorption curves at 140 °C under 0.1 MPa H_2 pressure obtained for a ball milled $LiAlH_4$ + 5 wt.% n-Ni mixture after long-term storage at room temperature (RT) for varying number of days.

time at RT. That means that a substantial desorption of H_2 occurred due to a slow decomposition of ball milled n-Ni catalyzed $LiAlH_4$ at RT. Similar volumetric curves were obtained after long-term storage at 40 and 80 °C and all of them were used to construct plots of hydrogen desorbed (wt.%) vs. storage time at RT, 40 and 80 °C which are shown in Fig. 13. Fig. 13a shows that the amount of H_2 desorbed decreases nearly linearly from initial ~7.2 wt.% to about 3.8 wt.% within 25 days of storage at RT. That means that about 3.4 wt.%H_2 was already released within 25 days of storage at RT. For storage over 25 days at RT the microstructure stabilizes and the release of H_2 somehow subsides. However, as shown in Fig. 13b increase of storage temperature to 40 °C accelerates slow desorption of H_2 to the extent that after 20 days the amount of desorbed H_2 decreases from initial ~7.6 to ~3.0 wt.% which means that the mixture desorbed about 4.6 wt.%H_2 during storage for 20 days at 40 °C. As shown in Fig. 13c increase of storage temperature to 80 °C leads to much faster desorption of H_2 to the extent that for a mixture catalyzed with 5 wt.% n-Ni the desorbed amount of H_2 drops rapidly from the initial ~7.4 to ~2.7 wt.% within barely 1 day (24 h) of storage and then slowly decreases nearly linearly when storage time increases to 30 days. Hence, within the first day of storage the mixture is able to desorb ~4.7 wt.%H_2 and additional 0.7 wt.%H_2 within the next 29 days. The increase of the n-Ni content to 10 wt.% does not increase the rate of slow desorption within the first day of storage but slightly accelerates the rate of slow desorption for storage over 1 day (Fig. 13c).

It is apparent that n-Ni is a very potent catalyst destabilizing a ball milled mixture of $LiAlH_4$ + 5 or 10 wt.% to the extent that it is capable to desorb slowly large amounts of hydrogen at RT, 40 and 80 °C. The rate of H_2 release during storage can be easily regulated by increasing or decreasing temperature. The range of temperatures and quantities of H_2 desorbed are close to the revised Department of Energy (D.O.E.) targets for 2015 for hydride desorption [22]. These virtues make the $LiAlH_4$ + 5 wt.% n-Ni mixture a potential hydrogen storage material for applications where a continuous supply of hydrogen is required for a prolonged service time as, for example, in some chemical processes where the presence of a reducing atmosphere is required. Other applications such as supply of the fuel cells for small electronic goods or automotive is more problematic. As argued by Graetz and Reilly [23] for a kinetically stabilized hydride such as catalyzed $LiAlH_4$ a hydrogen storage tank design would have to accommodate slowly desorbed excess H_2 using, for example, a hybrid high pressure/metal hydride option.

In order to understand the microstructural evolution which occurs during slow desorption at various temperatures the XRD samples were extracted after various storage time at a constant temperature. Fig. 14 shows XRD patterns obtained from a $LiAlH_4$ + 5 wt.% n-Ni mixture milled under IMP68 for 15 min and stored at RT for 25 and 65 days. It is clear that the microstructure after 25 days consists mainly of a mixture of retained $LiAlH_4$, newly formed Li_3AlH_6 and Al. This kind of microstructure confirms that reaction (4) was incomplete during storage at RT which also agrees well with the release of ~3.4 wt.%H_2 as discussed above. It is also seen that this microstructure is not changed after 65 days

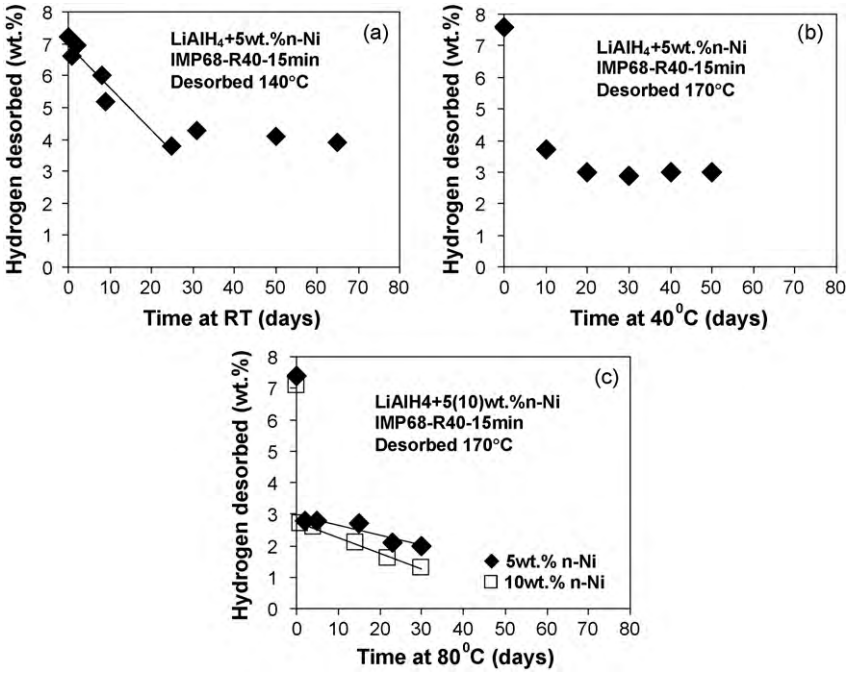

Fig. 13. Plots of hydrogen desorbed vs. storage time in days (1 day = 24 h) for $LiAlH_4$ + 5(10) wt.% n-Ni mixtures ball milled for 15 min under high energy IMP68 mode with R40. (b) Stored at room temperature (RT) under Ar; subsequently desorbed at 140 °C under 0.1 MPa H_2 pressure. (c) Stored at 40 °C under Ar; subsequently desorbed at 170 °C under 0.1 MPa H_2 pressure. (d) Stored at 80 °C under Ar; subsequently desorbed at 170 °C under 0.1 MPa H_2 pressure.

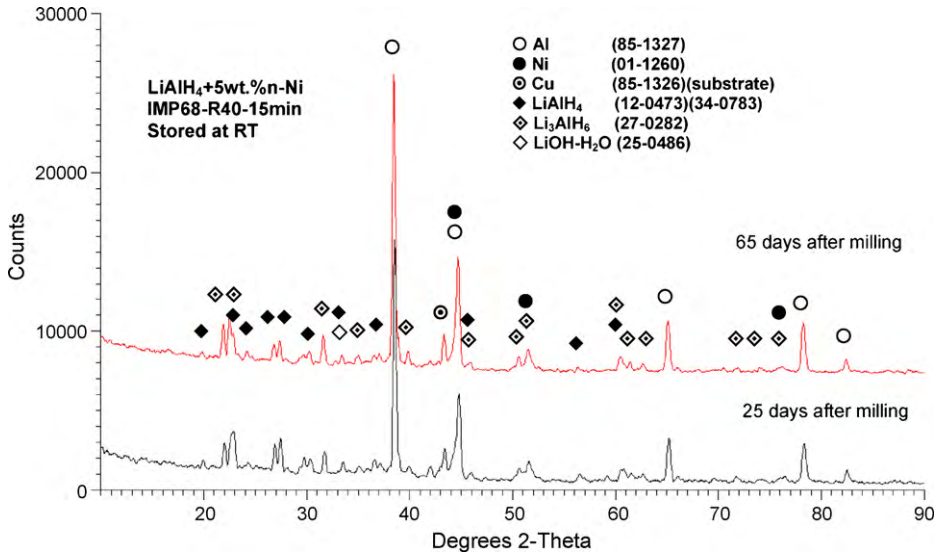

Fig. 14. XRD patterns obtained from a $LiAlH_4$ + 5 wt.% n-Ni mixture milled under IMP68 for 15 min with R40 and stored at RT under Ar for 25 and 65 days (1 day = 24 h).

of storage which is in excellent agreement with Fig. 13a showing a nearly no release of hydrogen during storage between 25 and 65 days. For comparison, at 80 °C as shown in Fig. 15, after 15 days of storage the microstructure consists mainly of newly formed Li_3AlH_6, Al and possibly some small amount of LiH a part of which is hydrolyzed/oxidized to LiOH. This microstructure indicates near completion of reaction (4) and the beginning (possibly) of reaction (5). After 30 days the microstructure consists of a minimal amount of retained Li_3AlH_6 (see very weak peaks on the verge of resolution), mostly Al and some LiH whose 100% peak is clearly visible in the form of a "shoulder" observed at the foot of the (2 0 0) Al peak ($2\theta = 44.70°$).

3.5. Rehydrogenation attempts

The reported results of the attempts to rehydrogenate catalyzed $LiAlH_4$ in which the catalytic addition might somehow alter unfavorable conditions for reversibility are conflicting. Wang et al. [24] tried to directly rehydrogenate $LiAlH_4$ doped with $TiCl_3$ under ~8 MPa of hydrogen pressure at 125 °C. Liu et al. [4] attempted to rehydrogenate under 95 bar of H_2 at 20, 50, 100, 150 and 200 °C. No successful rehydrogenation occurred. On the other hand, already cited Chen et al. [19] and Hima Kumar et al. [20] reported partial rehydrogenation of $LiAlH_4$ doped with 2 mol% $TiCl_3$–1/3$AlCl_3$ and 5 wt.% CNF (carbon nanofibers) under 40 bar/175 °C and 20 bar/110 °C.

Following these attempts, we also made a few attempts to rehydrogenate already dehydrogenated $LiAlH_4$ + 5 wt.% n-Ni which was ball milled under IMP68, R132 for 15 min as listed in Table 2. The rehydrogenation trials were conducted in our Sieverts-type apparatus immediately after dehydrogenation step. The dehydrogenation temperatures were selected in such a manner as to try rehydrogenation either starting from the (Li_3AlH_3 + Al) (dehydrogenation at 120 °C) or from (LiH + Al) (dehydrogenation at 170 and 250 °C) phase composition in accord with the reversed reaction (4) or (5), respectively. The microstructure after dehydrogenation was investigated by XRD of samples which were separately dehydrogenated at a selected temperature. The result of rehydrogenation

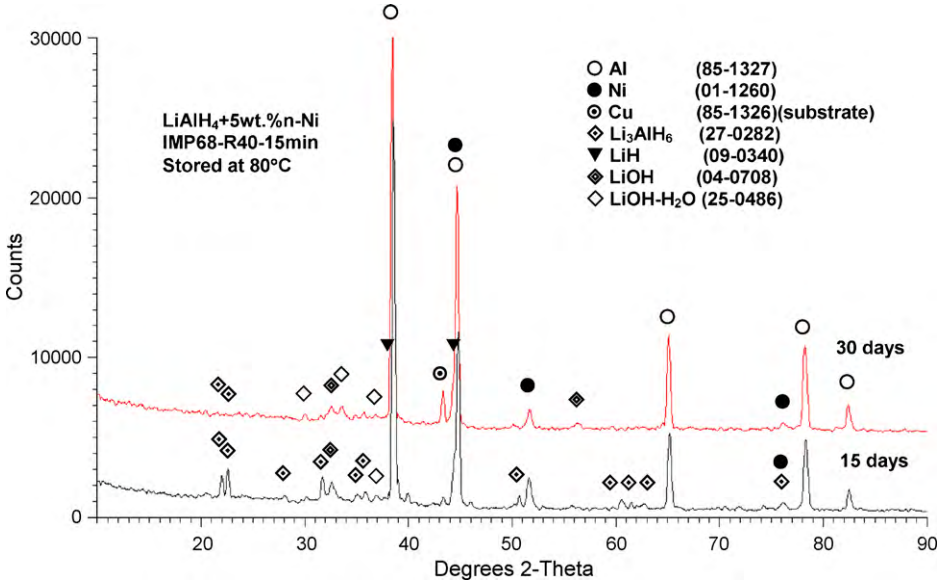

Fig. 15. XRD patterns obtained from a $LiAlH_4$ + 5 wt.% n-Ni mixture milled under IMP68 for 15 min with R40 and stored at 80 °C under Ar for 15 and 30 days (1 day = 24 h).

Table 2
Rehydrogenation studies for $LiAlH_4$ + 5 wt.% n-Ni ball milled IMP68, R132, 15 min.

Dehydrogenation			Rehydrogenation			
Temperature (°C)	Time (s)	Phases present	Temperature (°C)	Time (h)	Pressure (MPa)	Phases present or desorption behavior
120	1700	Li_3AlH_6, ($LiAlH_4$), (LiH) Al, Ni	55	64	5.2	Li_3AlH_6, ($LiAlH_4$), (LiH), Al, Ni
120	1400	Li_3AlH_6, ($LiAlH_4$), (LiH) Al, Ni	140	3.5	5.2	Li_3AlH_6, (LiH), Al, Ni
120	1600	Li_3AlH_6, ($LiAlH_4$), (LiH) Al, Ni	250	2	5.0	LiH, Al, Ni
170	3500	LiH, Al, Ni	55	18.5	5.2	No desorption at 170 °C after rehydrogenation
170	7500	LiH, Al, Ni	70	14	10.0	No desorption at 170 °C after rehydrogenation
250	1300	LiH, Al, Ni	200	12	0.2	LiH, Al, Ni
250	1300	LiH, Al, Ni	250	12	5.0	LiH, Al, Ni

Comment: A minority phase is given in parentheses.

was investigated by either removing a sample from the reactor and placing it in the environmental holder in a glove box and taking XRD of the microstructure or by conducting desorption studies immediately after the rehydrogenation step to monitor if there is any hydrogen release. In the latter case a sample was not removed from the reactor after rehydrogenation step but was immediately subjected to dehydrogenation procedure. Table 2 shows that there is no practical effect of rehydrogenation under the conditions applied in this study. It must, however, be pointed out that our Sieverts-type system can only achieve a maximum pressure of 10 MPa. Therefore, it is still unknown how the rehydrogenation process of n-Ni catalyzed $LiAlH_4$ would look like at the pressures higher than 10 MPa. There is still some room to maneuver here.

In general, pristine $LiAlH_4$ is considered for all practical purposes irreversible [1]. Computed stability diagram of LiH, Li_3AlH_6 and $LiAlH_4$ as presented in Fig. 3.12 in Ref. [1] (adopted from Ref. [25]) shows that at RT (298 K) the reversible reaction $Li_3AlH_6 \rightarrow LiAlH_4$ (reversed reaction (4)) would require a partial hydrogen pressure in excess of 10^3 bar while the reversible reaction $LiH \rightarrow Li_3AlH_6$ (reversed reaction (5)) would require a pressure from 10^{-2} to 10 bar. The reversibility of the latter seems to be more feasible. It must, however, be pointed out that the cited computations did not take into account any catalyzing additives.

However, Kojima et al. [26] reported that a small amount of $LiAlH_4$ could be directly synthesized by ball milling of LiH and Al in hydrogen which indicates a possibility of off board rehydrogenation of spent $LiAlH_4$. However, this approach has not been followed by more studies. Also, the most recent studies show [27] that dehydrogenated Ti-catalyzed $LiAlH_4$ can be relatively easily recharged off board under 10 MPa hydrogen pressure in dimethyl ether (Me_2O) as the reaction medium to stabilize the nascent $LiAlH_4$ formed during recharging. So in the worst case scenario, there are still some possibilities to recharge spent $LiAlH_4$ off board.

3.6. Flammability assessment

The addition of n-Ni does not change in any measurable way flammability of $LiAlH_4$ which was described in detail for pristine $LiAlH_4$ in Ref. [9]. It means that $LiAlH_4$ + n-Ni is a relatively benign hydride not really prone to self-ignition on contact with air that may contain some amount of moisture.

4. Conclusions

(1) No decomposition during milling up to 1 h has been observed for a $LiAlH_4$ + 5 and 10 wt.% n-Ni system.
(2) A doping of $LiAlH_4$ with n-Ni by a simple mixing still results in the endothermic melting of $LiAlH_4$ in a DSC test.
(3) Doping with 5 and 10 wt.% n-Ni combined with low energy ball milling (low energy shearing-LES) still leaves some trace of endothermic $LiAlH_4$ melting on a DSC curve.
(4) High energy ball milling under strong impact mode of $LiAlH_4$ + 5 wt.% n-Ni completely eliminates melting of $LiAlH_4$ in a DSC test.
(5) The decomposition reaction in DSC of n-Ni ball milled catalyzed $LiAlH_4$ occurs fully in a solid state according to the following reaction: $LiAlH_4$ (solid) → 1/3Li_3 AlH_6 (solid) + 2/3Al (solid) + H_2, at a temperature range much lower than its melting point as a result of an enormous acceleration of decomposition process by doping with a n-Ni catalytic additive; however, the character of this reaction is still exothermic.
(6) Volumetric dehydrogenation studies under 0.1 MPa H_2 pressure show that throughout the entire temperature range from 100 °C to 160 °C a $LiAlH_4$ + n-Ni nanocomposite system ball milled under high energy mode always desorbs hydrogen *in a solid state* in two stages I and II. Stage I is related to the transformation of $LiAlH_2$ into Li_3AlH_6 + Al + H_2 and stage II is related to the transformation of Li_3AlH_6 into LiH + Al + H_2. The apparent activation energy of Stage I and II is estimated as being equal to ~70 and ~100 kJ/mol, respectively. The former is much lower that the apparent activation energy reported for metal chloride catalysts.
(7) Ball milled mixture of $LiAlH_4$ + 5 wt.% n-Ni is capable to desorb slowly large quantities of hydrogen at RT, 40 and 80 °C owing to the strong catalytic action of n-Ni.
(8) No successful rehydrogenation has been observed under conditions of 55–250 °C and 0.2–10 MPa H_2.

Acknowledgments

This research was supported by the NSERC Hydrogen Canada (H2CAN) Strategic Research Network, NSERC Discovery and NSERC/Vale Inco Inc. Collaborative Research and Development grants which are gratefully acknowledged. The authors would like to thank Dr. Vladimir Paserin and Mr. Steve Baksa of Vale Inco Ltd. for producing and supplying the nanometric Ni powder used in this study. The authors are grateful to Prof. Linda Nazar from the Department of Chemistry, University of Waterloo, for the usage of XRD equipment.

References

[1] R.A. Varin, T. Czujko, Z.S. Wronski, Nanomaterials for Solid State Hydrogen Storage, Springer Science+Business Media, New York, NY, 2009.
[2] J.R. Ares Fernandez, F. Aguey-Zinsou, M. Elsaesser, X.Z. Ma, M. Dornheim, T. Klassen, R. Bormann, Int. J. Hydrogen Energy 32 (2007) 1033–1040.
[3] H.W. Brinks, A. Fossdal, J.E. Fonneløp, B.C. Hauback, J. Alloys Compd. 397 (2005) 291–295.
[4] S. Liu, L. Sun, Y. Zhang, F. Xu, J. Zhang, H. Chu, M. Fan, T. Zhang, X. Song, J.P. Grolier, Int. J. Hydrogen Energy 34 (2009) 8079–8085.
[5] M. Ismail, Y. Zhao, X.B. Yu, S.X. Dou, Int. J. Hydrogen Energy 35 (2010) 2361–2367.
[6] V.P. Balema, J.W. Wiench, K.W. Dennis, M. Pruski, V.K. Pecharsky, J. Alloys Compd. 329 (2001) 108–114.
[7] M. Resan, M.D. Hampton, J.K. Lomness, D.K. Slattery, Int. J. Hydrogen Energy 30 (2005) 1413–1416.

[8] Y. Kojima, Y. Kawai, M. Masumoto, T. Haga, J. Alloys Compd. 462 (2008) 275–278.
[9] R.A. Varin, L. Zbroniec, J. Alloys Compd. 504 (2010) 89–101.
[10] V. Paserin, S. Baksa, A. Zaitsev, J. Shu, F. Shojai, W. Nowosiadly, J. Nanosci. Nanotechnol. 8 (2008) 4049–4055.
[11] A. Calka, A.P. Radlinski, Mater. Sci. Eng. A 134 (1991) 1350–1353.
[12] Patents WO9104810, US5383615, CA2066740, EP0494899, AU643949.
[13] A. Calka, R.A. Varin, in: T.S. Srivatsan, R.A. Varin, M. Khor (Eds.), Int. Symp. on Processing and Fabrication of Advanced Materials IX (PFAM IX), ASM International, Materials Park, OH, 2001, pp. 263–287.
[14] H.P. Klug, L. Alexander, X-ray Diffraction Procedures for Polycrystalline and Amorphous Materials, John Wiley & Sons, New York, 1974, pp. 618–708.
[15] A. Calka, A.P. Radlinski, Mater. Sci. Eng. 97 (1988) 241–246.
[16] J. Block, A.P. Gray, Inorg. Chem. 4 (1965) 304–305.
[17] A. Andreasen, J. Alloys Compd. 419 (2006) 40–44.
[18] D. Blanchard, H.W. Brinks, B.C. Hauback, P. Norby, J. Muller, J. Alloys Compd. 404–406 (2005) 743–747.
[19] J. Chen, N. Kuriyama, Q. Xu, H.T. Takeshita, T. Sakai, J. Phys. Chem. B 105 (2001) 11214–11220.
[20] L. Hima Kumar, B. Viswanathan, S. Srinivasa Murthy, Int. J. Hydrogen Energy 33 (2008) 366–373.
[21] D. Blanchard, A.I. Lem, S. Øvergaard, H.W. Brinks, B.C. Hauback, J. Alloys Compd. 458 (2008) 467–473.
[22] S. Dillich, 2009 DOE Hydrogen Program & Vehicle Technologies Program, May 19, U.S. Department of Energy, 2009.
[23] J. Graetz, J.J. Reilly, Scripta Mater. 56 (2007) 835–839.
[24] J. Wang, A.D. Ebner, J.A. Ritter, Adsorption 11 (2005) 811–816.
[25] J.W. Jang, J.H. Shim, Y.W. Cho, B.J. Lee, J. Alloys Compd. 420 (2006) 286–290.
[26] Y. Kojima, Y. Kawai, T. Haga, M. Matsumoto, A. Koiwai, J. Alloys Compd. 441 (2007) 189–191.
[27] X. Liu, G.S. McGrady, H.W. Langmi, C.M. Jensen, J. Am. Chem. Soc. 131 (2009) 5032–5033.